Journal of Molecular Structure 1199 (2020) 127007

Contents lists available at ScienceDirect

Journal of Molecular Structure

journal homepage: http://www.elsevier.com/locate/molstruc

New pyrazolo-triazolo-pyrimidine derivatives as antibacterial agents: Design and synthesis, molecular docking and DFT studies

Mabrouk Horchani [a], Amel Hajlaoui [a], Abdel Halim Harrath [b], Lamjed Mansour [b], Hichem Ben Jannet [a], Anis Romdhane [a, *]

[a] Laboratory of Heterocyclic Chemistry, Natural Products and Reactivity (LR11Es39), Team: Medicinal Chemistry and Natural Products, Faculty of Science of Monastir, University of Monastir, Avenue of Environment, 5019, Monastir, Tunisia
[b] King Saud University, Department of Zoology, College of Science, Riyadh, Saudi Arabia

ARTICLE INFO

Article history:
Received 21 June 2019
Received in revised form
27 August 2019
Accepted 29 August 2019
Available online 30 August 2019

Keywords:
Pyrazolo-triazolo-pyrimidine
Antibacterial
Molecular docking
DFT

ABSTRACT

A new series of antibacterial pyrazolo-triazolo-pyrimidine derivatives **3a-3i** were synthesized in two steps starting from aminopyrazole **1** and characterized by ^{1}H NMR ^{13}C NMR and HRES-MS. Their molecular geometry are also calculated by the Density Functional Theory (DFT) employing B3LYP level with 6-311G (d,p) basis set. All the synthesized compounds were tested for *in vitro* antibacterial activity against a panel of selected bacterial strains, by application of the Disc-Diffusion and MIC assays, using gentamicin as standard. The interactions of these compounds with the bacteria *Pseudomonas aeruginosa* (LasR) were performed by molecular docking studies.

1. Introduction

Heterocycles have been found a key structural in medical chemistry and also they are frequently found in large percent in biomolecules such as enzyme, vitamins, natural products and biological active compounds. In this context, and as commonly reported that the presence of two or more heterocyclic pharmacophores linked and/or fused within a same structure generally could contribute to provide a significant positive effect on the overall biological efficiency in the resulting poly-heterocycle [1], we have oriented our research to prepare new classes of heterocyclic compounds associating within a same scaffold the pyrazole, the pyrimidine and the triazole moieties.

Indeed and as reported in literature, pyrazole and its derivatives are considered a pharmacologically important active scaffold that possesses almost all types of pharmacological activities particularly, they are described as anti-HCV [2], antitumor [3], cytotoxic [4], antioxidant [5] as well as antibacterial agents (Fig. 1A) [6].

On the other hand, pyrimidines, are widely found as the core structure in a large variety of compounds of great biological and pharmaceutical value exhibiting anticancer [7], antiviral [8], anti-inflammatory [9] and antibacterial activities (Fig. 1B) [10].

Finally, triazole and its derivatives have attracted the interest of medicinal chemists due to their broad spectrum of applications in medicinal chemistry and biochemical [11]. Thus, there are known as anti-tumoral [12] anticholinesterase [13], anti-tyrosinase [14], cytotoxic [15] and antibacterial (Fig. 1C) [16] agents.

On the other hand, and as reported, some works prove that DFT/B3LYP method has been commonly preferred to study structure, (QSAR) and many properties of organic molecules, because this method is efficient and offers an excellent trade-off between chemical accuracy, biological activity and computational cost [17–20].

These observations prompted us to synthesize some new poly-heterocycles bearing in their structures fragments described as antibacterial agents, as indicated above, such as pyrazole, pyrimidine and triazole derivatives and to investigate their antibacterial activity against two Gram-positive and four Gram-negative strains. Further molecular docking studies were carried out to include the drug-receptor interactions. The new analogues have been theoretically investigated by applying density functional theory (DFT) to understand the structure activity relationship.

* Corresponding author. Tel.: + 216 73 500 279; Fax: + 216 73 500 278
E-mail addresses: anis_romdhane@yahoo.fr, romdhaneanis.1@gmail.com (A. Romdhane).

https://doi.org/10.1016/j.molstruc.2019.127007
0022-2860/

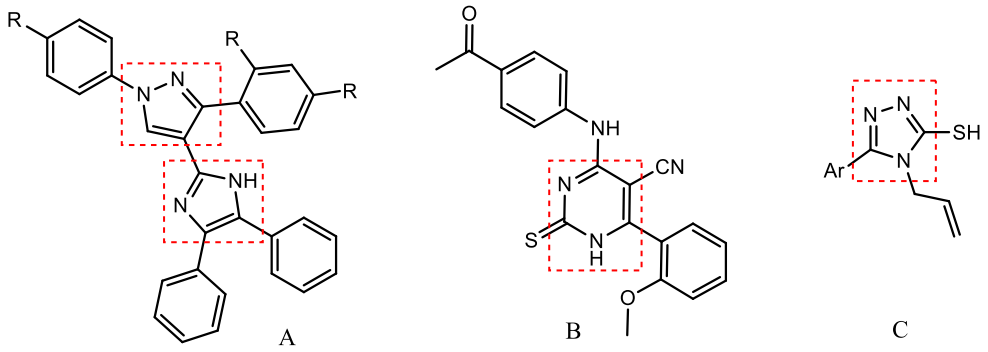

Fig. 1. Previously reported antibacterial nitrogen heterocycles.

2. Materials and methods

2.1. Materials

Melting points were determined on an Electrothermal 9002 melting point apparatus and are uncorrected. IR spectra were recorded on a FTS-6000 BIO-RAD apparatus. 1H NMR (300 MHz) and 13C NMR (75 MHz) spectra were recorded in deuterated $CDCl_3$ and DMSO-d_6 on a Bruker AC-300 using non deuterated solvents as internal reference. All chemical shifts were reported as δ values (ppm) and coupling constants (J) were expressed in Hz. High Resolution Mass Spectra (HRES-MS) were obtained with Micromass LCT (ESI technique, positive mode) spectrometers. All reactions were monitored by TLC using aluminum sheets of sds silica gel 60 F254, 0.2 mm. The starting materials **1** were prepared according to the literature [21].

2.2. Methods

2.2.1. General procedure of synthesis of ethyl (E)-N-(4-cyano-3-methyl-1-phenyl-1H-pyrazol-5-yl) formimidate

In a 250 mL flask equipped with a condenser, 0.1 mol of the precursor **1** and 0.12 mol of the triethyl orthoformate are poured in 150 mL of acetic anhydride; then the mixture is stirred under reflux. The mixture is allowed to return to room temperature and the reaction volume is reduced to half by the rotary evaporator. The mixture is then kept overnight in the refrigerator. The product obtained by filtration is then recrystallized from hexane.

2.2.1.1. Ethyl (E) -N- (4-cyano-3-methyl-1-phenyl-1H-pyrazol-5-yl) formimidate ***2***. Yellow solid; Yield (%) = 65; m.p (°C) = 78–80; ^{1}H NMR ($CDCl_3$,300 MHz): δ (ppm) = 1.36 (t, 3H, J = 7.2 Hz, H_{14}); 4.32 (q, 2H J = 6.9 Hz, H_{13}); 2,4 (s, 3H, H_7); 8,37 (s, 1H, H_{12}); 7.26–7.63 (m, 5H, H_{arom}); ^{13}C NMR ($CDCl_3$, 75 MHz): δ (ppm) = 12.5 (C_7); 13.4 (C_{14}); 63.7 (C_{13}+ C_4); 114.1 (CN); 123.4–137.6 (C_{arom}); 149.5 (C_5); 151.1 (C_3); 159.7 (C_{12}).

2.2.2. General procedure of synthesis of pyrazolotriazolopyrimidine derivatives *3*

In a 50 mL two-neck flask, 1 mmol of iminoether **2** is dissolved with 1.1 equivalents of hydrazide and a few drops of acetic acid in 40 mL of anhydrous dioxane. The mixture is stirred under reflux for 24 h, the solid formed by precipitation is filtered and then washed with petroleum ether.

2.2.2.1. 3a: 2-(9-methyl-7-phenyl-7H-pyrazolo[4,3-e] [1,2,4]triazolo [1,5-c]pyrimidin-2-yl) acetonitrile. White solid; Yield (%) = 52; m.p(°C) = >300; HRMS $[M+H]^+$ calcd. for $(C_{15}H_{11}N_7)^+$: 290.1154; found 290.1167; ^{1}H NMR (300 MHz, DMSO-d_6): δ (ppm) = 2.73 (s, 3H,H_{10}), 4.55 (s, 2H,H_{15}), 7.43 (t, 1H, J = 7.2 Hz, H_{14}), 7.59 (t, 2H, J= 7.5 Hz, $H_{13+}H_{13'}$), 8.09 (d, 2H, J = 7.8Hz, H_{12+} $H_{12'}$), 9,66 (s, 1H, H_5); ^{13}C NMR (75 MHz, DMSO-d_6): δ (ppm) = 18.6 (C_{10}), 23.1 (C_{15}), 107.9 (C_{9a}), 121.7 (C_{16}), 126.9–134.5 (C_{arom}), 143.2 (C_{11}), 145.5 (C_5), 147.8 (C_9), 151.4 (C_{9b}), 153.8 (C_2), 164.7 (C_{6a}).

2.2.2.2. 3b: 2,9-dimethyl-7-phenyl-7H-pyrazolo [4,3-e] [1,2,4] triazolo [1,5-c] pyrimidine. White solid; Yield (%) = 70; m.p (°C) = >300; HRMS $[M+H]^+$ calcd. for $(C_{14}H_{12}N_6)^+$: 265.1202; found 265.1211; ^{1}H NMR (300 MHz, $CDCl_3$): δ (ppm) = 2.68 (s, 3H. H_{10}), 2.87 (s, 3H, H_{15}), 7.39 (t, 1H, J = 7.2 Hz, H_{14}), 7.56 (dd, 2H, J_1= 7.5 Hz, J_2= 1.8 Hz, $H_{13+}H_{13'}$), 8.11 (d, 2H, J = 7.5 Hz, H_{12+} $H_{12'}$), 9.07 (s, 1H, H_5); ^{13}C NMR (75 MHz, $CDCl_3$): δ (ppm) = 13.8 (C_{10}), 14.6 (C_{15}), 102.2(C_{9a}), 122.1–129.2 (C_{arom}), 138.1 (C_{11}), 138.4 (C_5), 143.3(C_9), 146.4 (C_{9b}), 148.9 (C_{6a}), 165.8(C_2).

2.2.2.3. 3c: 9-methyl-2,7-diphenyl-7H-pyrazolo [4,3-e] [1,2,4] triazolo [1,5-c] pyrimidine. White solid; Yield (%) = 42; m.p (°C) = >300; HRMS $[M+H]^+$ calcd. for $(C_{19}H_{14}N_6)^+$: 327.1367; found 327.1378, ^{1}H NMR (300 MHz, $CDCl_3$): δ (ppm) = 2.93 (s, 3H, H_{10}), 7.28–8.37 (m, 10H, H_{arom}), 9.14 (s, 1H, H_5); ^{13}C NMR (75 MHz, $CDCl_3$): δ (ppm) = 13.3 (C_{10}); 103 (C_{9a}), 121.5 ($C_{12+}C_{12'}$), 126.6 (C_{14}), 127.2 ($C_{16+}C_{16'}$), 128.3 ($C_{17+}C_{17'}$), 128.7 ($C_{13+}C_{13'}$), 129.4 (C_{18}), 130.2 (C_{15}), 137.9 (C_{11}), 138 (C_5), 143 (C_9), 145.9 (C_{9b}), 148,7 (C_{6a}), 165.4 (C_2).

2.2.2.4. 3d: 9-methyl-7-phenyl-7H-pyrazolo [4,3-e] [1,2,4] triazolo [1,5-c] pyrimidine. White solid; Yield (%) = 38; m.p (°C) = 252–254; HRMS $[M+H]^+$ calcd. for $(C_{13}H_{10}N_6)^+$: 251.1045; found 251.1055; ^{1}H NMR (300 MHz, $CDCl_3$): δ (ppm) = 2.81 (s, 3H, H_{10}), 7.19–8.06 (m, 3H, H_{arom}), 8.05 (d, 2H, J = 7.5 Hz, $H_{12+12'}$), 8.33 (s, 1H, H_{15}), 9.10 (s, 1H, H_5); ^{13}C NMR (75 MHz, $CDCl_3$): δ (ppm) = 13.7 (C_{10}), 122.1 (C_{9a}), 124.1–129.9 (C_{arom}), 138.4 (C_5), 138.6 (C_9), 143.4 (C_{9b}), 148.4 (C_{6a}), 155.3 (C_2).

2.2.2.5. 3e: N-(9-methyl-7-phenyl-7H-pyrazolo[4,3-e] [1,2,4]triazolo [1,5-c]pyrimidin-2-yl)acetamide. White solid; Yield (%) = 41; m.p (°C) = 151–153; HRMS $[M+H]^+$ calcd. for $(C_{15}H_{13}N_7)^+$: 308.1282; found 308.1291; ^{1}H NMR (300 MHz, $CDCl_3$): δ (ppm) = 1.89 (s, 3H, H_{10}); 2.61 (s, 3H, H_{17}); 7.26 (t, 1H, J = 7.2 Hz, H_{14}), 7.24–8.22 (m, 5H, H_{arom}); 8.24 (s, 1H, H_5); 11.92 (s, 1H(NH)); ^{13}C NMR (75 MHz, DMSO-d_6): δ (ppm) = 14.4 (C_{10}); 20.98 (C_{17}); 100.3 (C_{9a}); 120.2–138.9 (C_{arom}); 142.8 (C_5); 154.1 (C_9); 156.5 (C_{9b}+C_2); 158.6 (C_{6a}); 171.9(C_{16}).

2.2.2.6. 3f: 2-ethoxy-9-methyl-7-phenyl-7H-pyrazolo [4,3-e] [1,2,4] triazolo [1,5-c] pyrimidine. White solid; Yield (%) = 69; m.p

(°C) = 182–184; HRMS $[M+H]^+$ calcd. for $(C_{15}H_{14}N_6O)^+$: 295.1307; found 295.1319; ^1H NMR (300 MHz, $CDCl_3$): δ (ppm) = 1.27 (t, 3H, H_{16}, J = 6,9 Hz), 2.58 (s, 3H, H_{10}), 4.23 (q, 2H, H_{15}, J = 7,2 Hz), 7.28 (t, 1H, J = 7.8 Hz, H_{14}), 7.43 (t, 2H, J_1= 8.1 Hz, $H_{13+}H_{13'}$), 8.01 (d, 2H, J = 7.5 Hz, H_{12+} $H_{12'}$), 8.51 (s, 1H, H_5); ^{13}C NMR (75 MHz, $CDCl_3$): δ (ppm) = 14.4 (C_{10}), 14 (C_{16}), 62.6 (C_{15}), 100.6 (C_{9a}); 121.6–138.5 (C_{arom}), 141.3 (C_5), 154 (C_9), 155.9 (C_2), 157.3 (C_{9b}), 157.9 (C_{6a}).

2.2.2.7. 3g: 4-methyl-7-((9-methyl-7-phenyl-7H-pyrazolo[4,3-e] [1,2,4]triazolo[1,5-c]pyrimidin-2-yl)methoxy)- 2H-chromen-2-one. White solid; Yield (%) = 55; m.p (°C) = >300; HRMS $[M+H]^+$ calcd. for $(C_{24}H_{18}N_6O_3)^+$: 439.1519; found 439.1532; ^1H NMR (300 MHz, $CDCl_3$): δ (ppm) = 2.24 (s, 3H, H_{10}), 2.82 (s, 3H, $H_{9'}$), 5.42 (s, 2H, H_{15}), 6.08 (s, 1H, $H_{3'}$), 6.17.(d, 1H, J = 8.7 Hz, $H_{6'}$), 6.85 (t, 1H, J = 6 Hz, H_{14}), 6.84–8.14 (m, 4H, H_{arom}), 8.12 (d, 2H, J = 7.8 Hz, H_{12+} $H_{12'}$), 9.07 (s, 1H, H_5); ^{13}C NMR (75 MHz, $CDCl_3$): δ (ppm) = 13.9 (C_{10}), 18.6 ($C_{9'}$), 29.7 (C_{15}), 64.1 ($C_{8'}$), 67.1 (C_{9a}), 102.2 ($C_{6'}$), 12.5 (C_{4a}); 112.8 ($C_{3'}$), 114.3 (C_{13}+$C_{13'}$), 122.2 ($C_{5'}$), 125.7 (C_7), 127.4 (C_{14}+$C_{14'}$), 129.2 (C_{12}), 138.3 (C_5), 138.4 (C_9), 143.5 (C_{9b}), 149.3 (C_2), 152.3 ($C_{6'a}$), 155.1 ($C_{4'}$), 161.1 ($C_{8'a}$), 163.6 ($C_{2'}$).

2.2.2.8. 3h: 2-(4-chlorophenyl)-3-((9-methyl-7-phenyl-7H-pyrazolo [4,3-e] [1,2,4]triazolo[1,5-c]pyrimidin-2-yl) methyl) quinazolin-4(3H)–one. White solid; Yield (%) = 65; m.p (°C) = 200–202; HRMS $[M+H]^+$ calcd. for $(C_{28}H_{19}ClN_8O)^+$: 519.1460; found 519.1469; ^1H NMR (300 MHz, $CDCl_3$): δ (ppm) = 2.89 (s, 3H, H_{10}), 6.07 (s, 2H, H_{15}), 7.25–8.55 (m, 13H, H_{arom}), 9.11 (s, 1H, H_5); ^{13}C NMR (75 MHz, $CDCl_3$): δ (ppm) = 14.2 (C_{10}), 56.2 (C_{15}), 102.4 (C_{9a}), 112.1 ($C_{12\ +}C_{12'}$), 119.9 ($C_{4'a}$), 121.9 (C_{14}), 123.2 ($C_{5'}$), 125 ($C_{9'}$), 125.2 ($C_{8'}$), 125.3 ($C_{6'}$), 125.4 ($C_{11''}$+$C_{11'''}$), 126.3 ($C_{10''}$+$C_{10'''}$), 128.5 (C_{13}+ $C_{13'}$), 129.2 ($C_{7'}$), 131.3 ($C_{12''}$), 133.5 (C_{11}), 134.3 (C_5), 139.5 (C_9), 15.6 (C_{9b}), 155.2 (C_2), 156.4 ($C_{8'a}$), 160 (C_{6a}), 167.7 ($C_{2'}$), 173.5 ($C_{4'}$).

2.2.2.9. 3i: 2-(4-methoxyphenyl)-3-((9-methyl-7-phenyl-7H-pyrazolo[4,3-e] [1,2,4]triazolo[1,5-c]pyrimidin-2-yl) methyl) quinazolin-4(3H)–one. White solid; Yield (%) = 43; m.p (°C) = 148–150; HRMS $[M+H]^+$ calcd. for $(C_{29}H_{22}N_8O_2)^+$: 515.1944; found 515.1955; ^1H NMR (300 MHz, $CDCl_3$): δ (ppm) = 2.9 (s, 3H, H_{10}), 3.89 (s, 3H, $H_{13''}$), 6.09 (s, 2H, H_{15}), 7.25–8.55 (m, 13H, H_{arom}), 9.12 (s, 1H, H_5); ^{13}C NMR (75 MHz, $CDCl_3$): δ (ppm) = 13.9 (C_{10}), 55.4 (C_{15}), 61.8 ($C_{13''}$), 103.5 (C_{9a}), 113.8 ($C_{11''}$+$C_{11'''}$), 114.7 (C_{12}+$C_{12'}$), 122.1 ($C_{9'}$), 123.7 ($C_{4'a}$), 126.2 (C_{14}), 127.3 ($C_{5'}$), 127.5 ($C_{8'}$), 129.2 ($C_{6'}$), 130.3 (C_{13}+$C_{13'}$), 133.8 ($C_{10''}$+$C_{10'''}$), 138.3 ($C_{7'}$), 138.4 (C_{11}), 143.4 (C_5), 146.3 (C_9), 149.1 (C_2), 151.9 (C_{9b}), 159.5 ($C_{8'a}$), 161.0 (C_{6a}), 164.3 ($C_{2'}$), 165.8 ($C_{4'}$), 179.3 ($C_{12''}$).

2.2.3. Antibacterial activity

2.2.3.1. Bacterial srains. The in *vitro* antibacterial activity of the synthesized compounds were assayed against six microorganisms, included four Gram-negative rods: *Escherichia coli* (ATCC 25922), *Pseudomonas aeruginosa* (ATCC 27853), *Citrobacter freundii* (clinical strain), *Proteus mirabilis* (clinical strain), and two Gram-positive cocci: *Staphylococcus aureus* (ATCC 25923) and *Enterococcus faecalis* (ATCC 29212) (American Type Culture Collection, Rockville, MD). The microbial strains were obtained from the culture collection of the Laboratory of Infectious Diseases and Biological Active Agents, Faculty of Pharmacy, Monastir, Tunisia.

2.2.3.2. Disc-Diffusion assay. The antibacterial activity of the prepared compounds was evaluated with the disc diffusion method using Mueller Hinton Agar (MHA). Inocula were prepared by diluting overnight (24 h at 37 °C) cultures in Muller Hinton Broth medium to approximately 10^6 colony-forming unit per milliliter (CFU/mL). Absorbent discs (diameter 6 mm, Whatman Paper No. 3) were impregnated with 10 μL of each sample dissolved 10% DMSO solution (in water) at the concentration of 100 μM and then placed on the surface of the inoculated plates (90 mm diameter). The plates were kept at 4 °C for 2 h before incubation at 37 °C for 24 h [22]. Then the diameters of the inhibition zones were measured. Positive control discs of gentamicin (10 μg/disc, Bio-Rad), were included in each assay, and the developing inhibition zones were compared with those of the reference disc. The 10% DMSO solution was also tested as negative control. The assays were performed in triplicate.

2.2.3.3. Micro-well dilution assay. The minimal inhibition concentration (MIC) values for the antibacterial activity were determined with the dilution method following the procedure described by Jabrane et al. [23]. The samples were prepared at a concentration of 1000 μM 10% DMSO solution. Sterile 10% DMSO solution (100 μL) was pipetted into all wells of the microtitre plate before transferring 100 μL of stock solution to the microplate and applying a series of dilutions. Finally, 50 μL of 10^6 colony forming units (cfu/mL) (according to Mc-Farland turbidity standards) of standards microorganism suspensions were inoculated on to microplates and incubated at 37 °C between 18 and 24 h. At the end of incubation period, the plates were evaluated for the presence or absence of growth. All the samples were screened three times against each microorganism. Gentamicin was used as antibacterial positive control.

2.2.4. Computational details (DFT studies)

The DFT calculations were performed using Gauss View 5 and GAUSSIAN 09 [24,25]. The molecular structure of the compounds in the ground state is optimized by using B3LYP/6-311 + G(d,p) level of the theory. The most stable and reactive molecule is determined by using energy gap which is the difference between the HOMO-LUMO orbitals.

2.2.5. Molecular docking procedure

Automated docking was used to determine the orientation of inhibitors bound in the active site of *P. aeruginosa* (LasR). The three-dimensional structure of PDB (PDB: 2UV0) were obtained from the RSCB protein data bank [26]. The molecular docking of the chemical compounds- LasR binding site was performed using Autodock Vina software [27].

3. Results and discussion

3.1. Chemistry

Justification of much of the chemistry directed to the synthesis of the compounds comprising nitrogen at the rings fusion, is due to the application of compounds having interesting antibacterial properties in the domain of medicinal chemistry. In this respect and encouraged by some of our previous results [28–30] the aim of this work was to synthesis some pyrazolo-triazolo-pyrimidine derivatives **3** (Scheme 1) (see Scheme 2).

In order to achieve this aim, it was necessary to first synthesize the aminopyrazole **1** according to the previously reported method [21]. Our approach to the target systems **3** was started by the synthesis of the α-functionalized iminoether **2**. Herein, we are reporting a simple and scalable methodology for the one-pot synthesis of our key intermediate **2** (65% yield) *via* condensation reaction of the precursor **1** with triethyl orthoformate under reflux of acetic anhydride [31].

The structures of the above compounds were established on the basis of their ^1H and ^{13}C NMR spectral data.

Subsequently, the reaction of ethyl (*E*)-*N*-(4-cyano-3-methyl-1-phenyl-1*H*-pyrazol-5-yl) formimidate **2** with a series of hydrazides

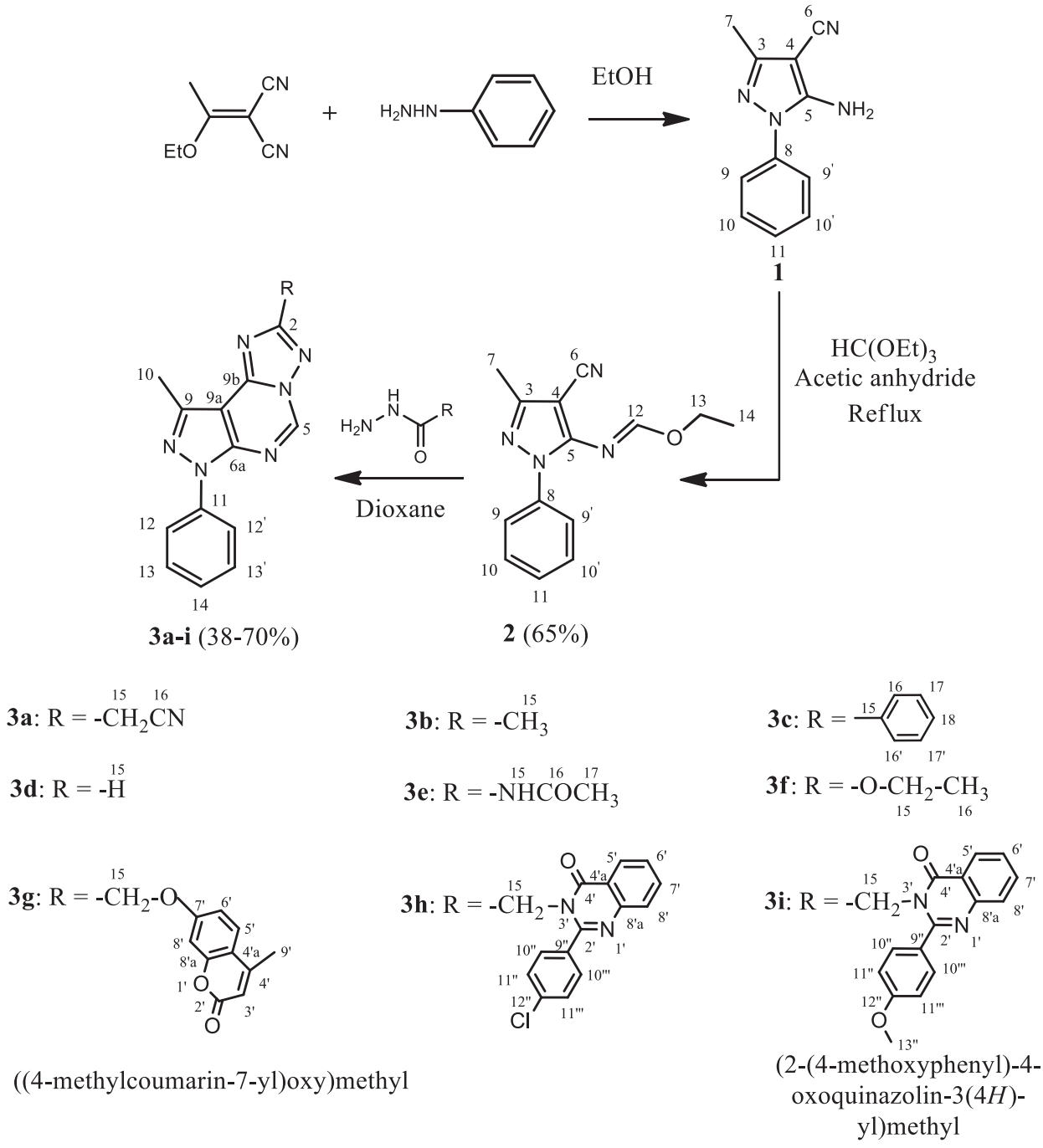

Scheme 1. Synthetic route of compounds **3a-3i**.

at reflux of dioxane leads to pyrazolo-triazolo-pyrimidine derivatives **3a-3i**. The use of a catalytic amount of acetic acid provided the product in reduced reaction time.Mechanistically, a first nucleophilic attack of the nitrogen doublet of the $-NH_2$ group on the iminoether's iminic carbon leads to the departure of an ethanol molecule. The obtained non isolable intermediate $\mathbf{I_1}$ undergoes an intramolecular cyclization following a second nucleophilic attack on the carbon of the nitrile function (CN) by the same nitrogen atom affording another intermediate $\mathbf{I_2}$, which gives, after intramolecular cyclization followed by a dehydration, the new pyrazolotriazolopyrimidine derivatives **3**, except of compound **3e** where the primary amine function was found acetylated with acetic acid in dioxane.

The structures of the new synthesized pyrazolo-triazolo-pyrimidine derivatives **3a-3i** were evidenced by their spectral data. The ^{1}H NMR spectra of these compounds showed the disappearance of signals related to methyl and methylene at δ_H 1.33–1.38 and 4.29–4.36, respectively, of the iminoether **2** and the observation of signals introduced by hydrazides. Unambiguous proofs for the obtained products **3a-3i** aroused from their ^{13}C NMR data, in

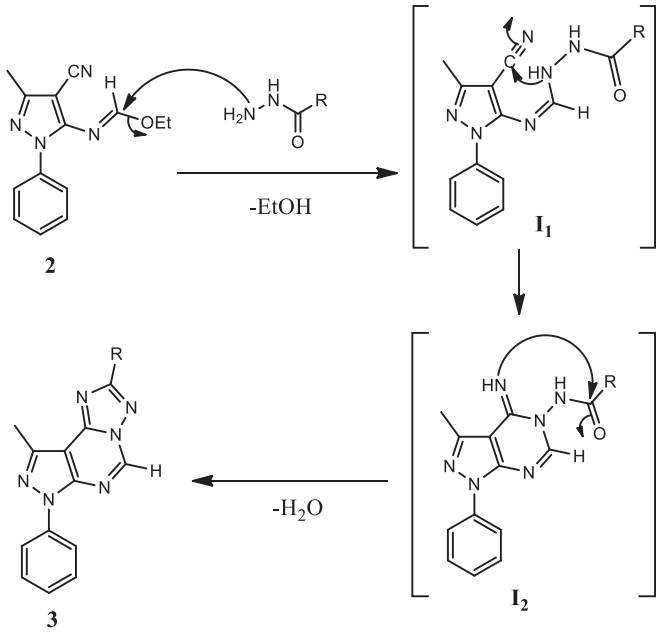

Scheme 2. Proposed synthetic pathway to compounds **3a-3i**.

fact, the spectra of these compounds showed essentially the appearance of a new signal at δ_C 149.1–165.8 due to the quaternary carbon C_2 introduced by the corresponding hydrazide and the disappearance of the signals relating to the carbons of the ethyl group (δ_C 13.4 and 63.7) and the nitrile function (δ_C 114.1).

In the same context and with regard to the compounds **3a**, **3g**, **3h** and **3i**, we noticed the presence of a signal in the zone (δ_C 23–56) which is reversed on the DEPT 135, attributable to the methylene group. This data is supported by the appearance of a singlet between δ_H 4.55 and 6.09 in the ^{1}H NMR spectrum. The assignment of several chemical shifts to protons and carbons constituting the products **3a-i** was supported by comparison with the literature [32,33].

Furthermore, the mass spectra (ES-HRMS) of compounds **3** showing the protonated molecular ion peaks $[M+H]^+$ where in good agreement with the assigned structures.

3.2. Biological activity

3.2.1. In vitro antibacterial bioassay

All the newly synthesized compounds were evaluated *in vitro* against an assortment of four Gram-negative (*Escherichia coli, Pseudomonas aeruginosa, Proteus mirabilis* and *Citrobacter freundii*) and two Gram-positive strains (*Enterococcus faecalis* and *Staphylococcus aureus*). The activity of all the tested compounds was compared with that of Gentamicin used as standard reference antibiotic (10 μg/disc), by measuring the inhibition zone (in mm). The inhibitory effects of compounds **1**, **2**, and **3a-3i** against these six strains are given in Table 1. The obtained results revealed that all synthesized compounds possess significant antibacterial activity against selected strains. The pyrazoles **1** and **2** were found to be moderately active only towards *P. mirabilis* and *C. freundii* (see Table 2).

On the other hand, the newly generated compounds **3a-3i** have exerted inhibitory activity against all of tested bacterial strains. Indeed, these compounds did not show a good activity towards Gram-positive bacteria (MIC≥ 400 μM) except the derivative **3h** with a (2-(4-chlorophenyl)-4-oxoquinazolin-3(4*H*)-yl)methyl moiety, which had a very interesting effect towards *S. aureus* (IZ = 23.5 ± 1 mm, MIC = 6.25 μM) compared to the other compounds and Gentamicin (IZ = 8.0 ± 0.8 mm). The data in Table 1 revealed that compounds **3a-3i** showed globally significant activity against the four Gram-negative bacteria used. Indeed, the compound **3i** showed the highest activity against *E. coli* with IZ and MIC values of 17.0 ± 0.6 mm and 12.5 μM, respectively. The noted inhibition zone of the same derivative was found to be comparable to that of gentamicin (17.5 ± 0.8 mm). Moreover, compounds **3d** (R = H), **3c** (R = Ph) and **3h** displayed good inhibitory results against the same strain (IZ = 15.1 ± 1.0, 15.9 ± 0.0 and 15.0 ± 0.0 mm, MIC = 50, 50 and 25 μM, respectively) whereas, compounds **3f** (R = OEt) and **3g** (R= ((4-methylcoumarin-7-yl)oxy) methyl) showed the lowest antibacterial potential. Furthermore, compound **3i** ((2-(4-methoxyphenyl)-4-oxoquinazolin-3(4*H*)-yl) methyl) was found to be the most active (IZ = 16.8 ± 1.0 mm, MIC = 12.5 μM) towards *P. mirabilis,* followed by compounds **3d** (R = H) and **3h** (IZ ≥ 15 mm and MIC = 25 μM). This result shows, in particular, the importance of the methoxy group in **3i** compared to the chlorine atom in **3h**. On the other hand, compounds **3** exhibited moderate to good activity (IZ ≥ 12 mm, MIC = 25–200 μM) against *C. freundii* compared to the reference antibiotic (11.8 ± 0.7 mm) except compound **3f** (IZ = 10.1 ± 0.6 mm, MIC = 400 μM). Most compounds **3a-3i** displayed noticeable antibacterial activity against *P. aeruginosa*. In this series, compound **3i** showed the highest activity (IZ = 16.8 ± 1.8 mm, MIC = 12.5 μM) and it was found slightly more active than the standard gentamicin (IZ = 16.0 ± 0.5 mm) followed by **3c**, **3d** and **3h**, respectively. It is worth to notice also that the molecules **3a** (R = CH_2CN), **3f** (R = ethoxy) and **3g** were found to be the less active ones against the same strain. All these observations clearly indicate that Gram-negative bacteria are more sensitive to compounds **3** than the gram-positive ones. This finding can be explained by a preferential interaction between these compounds and the cell wall of the Gram-negative strains which is composed of a single layer of peptidoglycan whereas in Gram-positive bacteria, the cell wall is thicker (15–80 nm) and consisting of several layers of peptidoglycan which could prevent any interaction with these types of compounds of a particular structure.

3.3. Molecular docking analysis of compound 3i

There are some previous studies that reported new inhibitors against *P. aeruginosa* (LasR) using in silico modeling of the ligand-receptor interaction in order to find a better inhibition efficiency [34]. Encouraged by this finding and to confirm the antibacterial effect of the synthesized compounds towards the used Gram-negative bacteria, especially *P. aeruginosa*, docking study into the crystal structure of *P. aeruginosa* (LasR) was employed. This bacteria has many potential sites where ligand can be bound. From the perspective of inhibitors, the most potent site is probably whose located in the proximity of residues taking key roles in catalytic functions. Before the docking, co-crystallized ligands and water molecules of each protein were removed, the molecular docking of the chemical compounds was performed using Autodock Vina software [27].

Molecular basis of interactions between target enzyme and the synthesized ligand **3i** (the most potent antibacterial) can be understood with the help of docking analysis and interactions as represented in Fig. 2.

In order to provide an explanation and understand the potent antibacterial activity of compound **3i**, it is pertinent to note that the later showed good docking interactions with the receptor site. Indeed, the pyrazolotriazolopyrimidine moiety exhibits the preferred bindings orientation. In this case, the triazole's nitrogen atom (position 3) showed a hydrogen bonding interaction to

Table 1
Antibacterial activities of compounds **1**, **2** and **3a-3i** expressed in Inhibition Zone (IZ).

Compound	Bacteria					
	Enterococcus faecalis ATCC 29212	*Staphylococcus aureus* ATCC 25923	*Escherichia coli* ATC	*Proteus mirabilis*	*Citrobacter freundii*	*Pseudomonas aeruginosa* ATCC 27853
Inhibition Zone (mm)						
1	-[a]	7.5 ± 0.2	–	8.0 ± 0.8	8.0 ± 1.0	–
2	–	8.0 ± 0.8	–	10.5 ± 0.7	11.5 ± 0.9	–
3a	8.5[b] ± 0.8	9.0 ± 0.1	12.5 ± 1.0	11.0 ± 1.0	12.0 ± 1.5	12.5 ± 1.0
3b	7.2 ± 0.5	9.5 ± 0.8	13.8 ± 1.0	11.8 ± 1.2	12.9 ± 1.0	14.5 ± 1.3
3c	8.5 ± 0.8	8.0 ± 0.4	15.1 ± 1.0	14.0 ± 1.0	13.7 ± 0.5	16.4 ± 1.0
3d	10.5 ± 0.1	7.5 ± 0.9	15.9 ± 0.0	15.0 ± 1.0	15.1 ± 0.9	15.4 ± 1.2
3e	9.0 ± 0.7	8.7 ± 0.4	13.5 ± 0.8	12.5 ± 1.3	13.1 ± 0.7	14.2 ± 1.0
3f	8.5 ± 0.8	7.5 ± 0.1	11.1 ± 0.8	11.0 ± 1.0	10.1 ± 0.6	10.0 ± 1.4
3g	9.0 ± 0.7	7.0 ± 0.7	11.5 ± 0.7	11.0 ± 1.1	12.3 ± 0.4	13.2 ± 1.0
3h	–	23.5 ± 1.0	15.0 ± 0.0	16.0 ± 1.5	15.0 ± 0.3	15.0 ± 0.6
3i	9.0 ± 0.8	7.5 ± 0.2	17.0 ± 0.6	16.8 ± 1.0	14.7 ± 0.9	16.8 ± 1.8
Gentamicin	20.5 ± 0.4	8.0 ± 0.8	17.5 ± 0.8	17.7 ± 1.2	11.8 ± 0.7	16.0 ± 0.5

ATCC: American Type Culture Collection.
Gentamicin: reference antibiotic (10 μg/disc).
[a] Inactive.
[b] Diameter of the Zone of Inhibition (IZ) expressed in mm including the disk (6 mm). The values are expressed in IZ ± standard deviation (number of repetitions = 3).

Table 2
Antibacterial activities of compounds **1**, **2** and **3a-3i** expressed in Minimum inhibitory concentration (MIC).

Compound	Bacteria					
	Enterococcus faecalis ATCC 29212	*Staphylococcus aureus* ATCC 25923	*Escherichia coli* ATCC 25922	*Proteus mirabilis*	*Citrobacter freundii*	*Pseudomonas aeruginosa* ATCC 27853
MIC (μM)						
1	>400	>400	>500	>500	>500	>500
2	>400	>400	>500	>500	>500	>500
3a	>400	400	100	400	200	100
3b	>400	400	100	200	100	50
3c	>400	>400	50	50	50	25
3d	400	>400	50	25	25	25
3e	>400	>400	50	100	100	50
3f	>400	>400	200	200	400	400
3g	400	>400	200	200	200	100
3h	>400	6.25	25	25	25	25
3i	400	>500	12.5	12.5	50	12.5

residue ASN-H-136 (green color). Moreover, in the pyrazolopyrimidine ring Pi −anion interactions were observed with GLU-H-139 (golden color). In addition, the methyl group linked to the pyrazole ring shows alkyl interactions with LEU-E-40, PHE-H-67 and PRO-E-41. Furthermore, the ((2-(4-methoxyphenyl)-4-oxoquinazolin-3(4*H*)-yl)methyl) introduced by hydrazide showed a Pi-Alkyl interaction with ALA-H-138 *via* its phenyl group and carbon-hydrogen bond with ASN-H-136 and ASP-E-46. Moreover, it is involved in conventional hydrogen bond interaction with SER-E-40 by its carbonyl focus. This finding clearly reveals that these interactions are the principle factor explaining the inhibition of *P. aeruginosa* by **3i** compared to the other derivatives.

3.4. DFT studies

DFT of chemical reactivity, which is titled conceptual DFT, is a relevant trait of the density functional language for defining and elucidating important chemical concepts of molecular structure and reactivity [35]. In this relation, quantum-chemical descriptors have been widely used in quantitative structure−activity relationship (QSAR) studies in biochemistry [36].

3.4.1. Frontier molecular orbitals analysis

In accordance with the frontier molecular orbital theory, HOMO and LUMO are the most substantial factors because these orbitals are indicator of molecular reactivity and properties. The orbital HOMO is capable to give electrons, while LUMO can take electrons first [37]. Fig. 3 shows the dispersion and energy levels of the HOMO and LUMO orbitals calculated at the B3LYP/6-311 + G(d,p).

As can be seen in Fig. 3a, the highest occupied molecular orbital (HOMO) is localized on the pyrazole fragment and CN function as well as NH_2 group. While the lowest unoccupied molecular orbital (LUMO) is localized on almost the entire structure except the methyl group. Otherwise, the HOMO orbital of the molecule **2** is confined on the benzene moiety, the pyrazole ring, the methyl group and partially on the NCHOEt moiety. The same for the LUMO orbital except for the methyl group as shown in Fig. 3b. On the other hand, in regards to in Fig. 3c, we note that the HOMO orbital bounded on the whole structure. In addition, the LUMO is centered on total structure unless the methyl group.

The difference between the HOMO-LUMO orbitals is known as energy gap. This energy range also allows to determine a kinetic stability, reactivity and chemical hardness-softness of a molecule reactivity [38,39]. Hard molecules with big HOMO-LUMO gap are more stable and less reactive. In the opposite case, soft molecules with small HOMO-LUMO gap are more reactive and less stable [40], in this context, Fig. 3 shows that aminopyrazole **1** has a large energy gap (5.06 eV) compared to iminoether **2** (4.59 eV). Moreover, the gap energy of the latter is greater than that of molecule **3d** (4,27eV), according to these data we can conclude that the

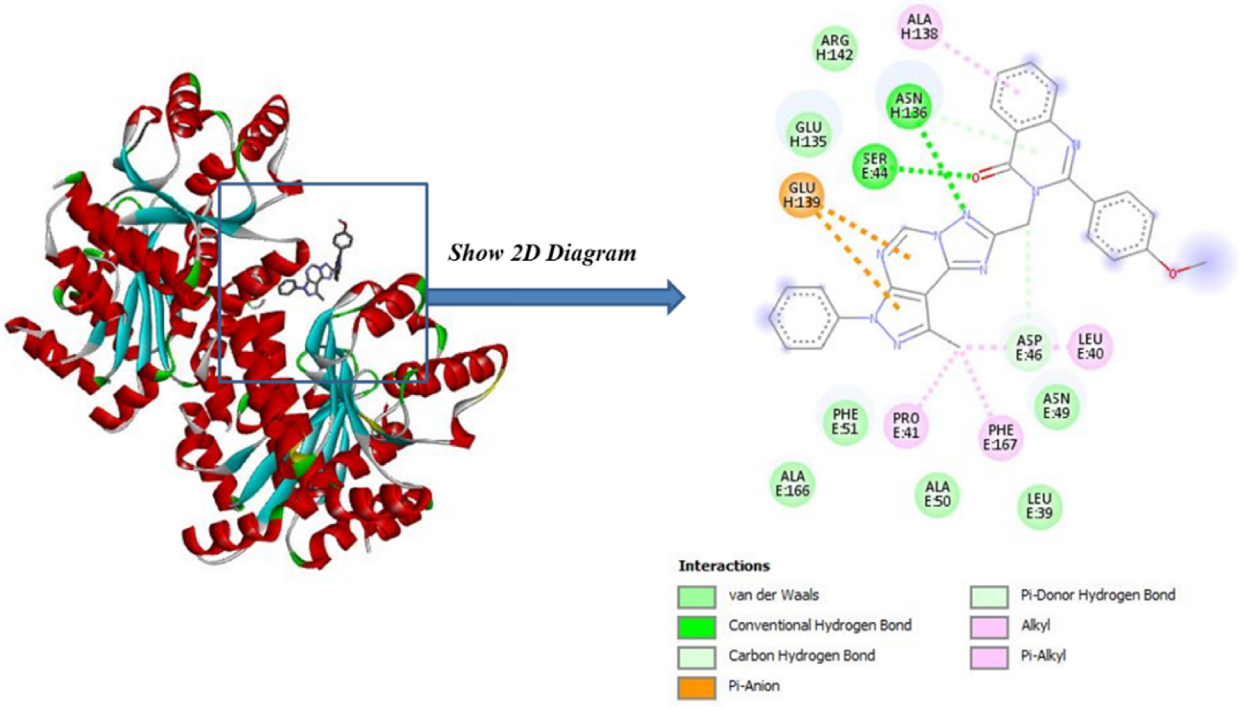

Fig. 2. Interaction of LasR receptor with compound **3i** (PDB: 2UV0).

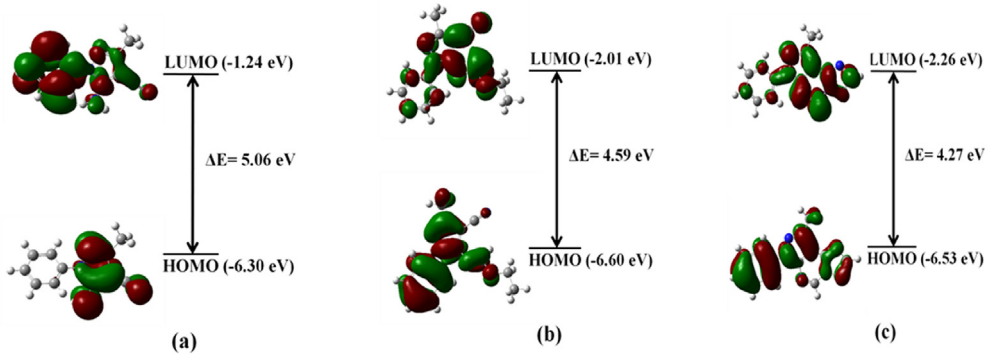

Fig. 3. Frontier Molecular Orbital of compounds **1** (a), **2** (b) and **3d** (c).

pyrazolotriazolopyrimidine derivative **3d** is softer and more reactive and less stable by comparison with the iminoether **2** who is also softer and more reactive and less stable than the aminopyrazole **1**. The low HOMO-LUMO gap supports the bioactive molecule [41–44]. In this context, compound **3d** giving a gap energy value lower than that of molecules **1** and **2**, has a significant antibacterial activity against most of the bacterial strains used. Therefore, heterocyclic molecules according to their softness have

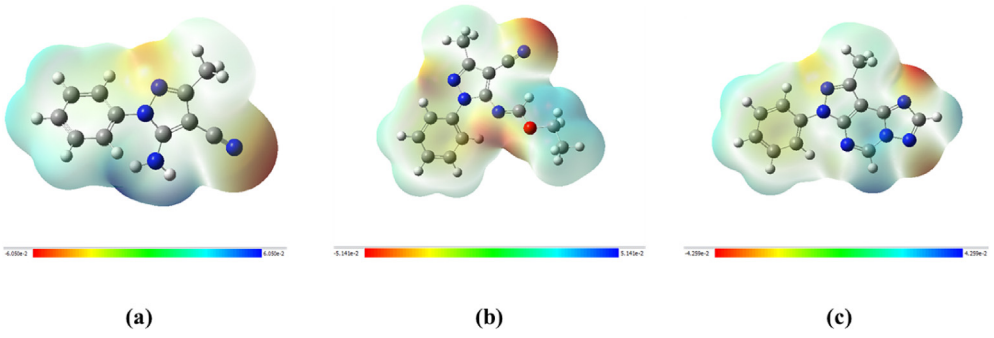

Fig. 4. Molecular Electrostatic Potential of compounds **1** (a), **2** (b) and **3d** (c).

an influence on the antibacterial activity.

3.4.2. Molecular electrostatic potential (MEP)

Molecular electrostatic potential (MEP) mapping gives information about the biological recognition process and hydrogen bonding interactions and helps to interpret the electrophilic and nucleophilic reactions [45]. The MEP of compounds **1**, **2** and **3d** is presented in Fig. 4. This property is used to predict the behavior and responsiveness of these molecules. In this case, to fully explain the mechanism of synthesis of compound **2** starting from the aminopyrazole **1**, we resort to the electrostatic potential in order to predict the reactive sites of electrophilic and nucleophilic attack for the investigated molecule, this theoretical calculation at the B3LYP/6-311 + G(d,p) optimized geometry of the synthesized compound **1** is used. The positive (blue) districts of MEP were related to nucleophilic reactivity while the negative (red and yellow) regions explain the electrophilic reactivity [46,47]. As we can see in Fig. 4a, the MEP of compound **1** has a single blue zone which is observed around the nitrogen atom linked to two hydrogen atoms. Therefore, it has a high electron density, so its free doublet is apt to attack electrophilic sites preferentially. Indeed, by double nucleophilic attack on triethyl orthoformate's electrophilic site, we obtain the iminoether **2**. On the other hand, the MEP of compound **2** shows that the most negative regions are located around the iminic carbon (linked to the ethoxy group) and the carbon of the nitrile function (CN), these atoms are likely to be attacked by the nitrogen-free doublet of the hydrazide, to train the pyrazolo-triazolo-pyrimidine derivatives **3a-3i**. In Fig. 4c the MEP of compound **3d** shows many negative regions in the investigated molecule which is explained by its large size. This electrostatic potential plays an important role to clarify, inter/intra-molecular interactions, drug-protein interactions and structure-activity relationship, the negative potential (red-yellow colored) is localized over the hydrogen atom of the pyrimidine ring in compound **3d** while the positive electrostatic potential (blue colored) is localized over the tow nitrogen atoms of the triazole group, these group regions may be well involved in the inhibition of bacteria.

4. Conclusion

In conclusion, this work reports the valorization of iminoether **2** as a pyrazole derivative, to access to new antibacterial pyrazolo-triazolo-pyrimidines derivatives **3a-3i**, *via* cyclocondensation reaction with hydrazides. The formed compounds have been tested *in vitro* for their possible antibacterial activities using the Disc-Diffusion and MIC assays. The molecular docking studies and DFT calculations proved that heterocyclic molecules incorporating, in the same time, pyrazole, triazole and pyrimidine moieties have an interesting antibacterial activity towards Gram-negative strains. It has been found that compound **3i** with a ((2-(4-methoxyphenyl)-4-oxoquinazolin-3(4*H*)-yl)methyl) moiety was able to inhibit *P. aeruginosa* one of the most resistant bacteria and this result was supported by significant binding interactions proven with in silico docking studies.

By DFT/B3LYP method with 6-311G+(d,p) level of theory, HOMO-LUMO gaps and molecular electrostatic potential have been examined and discussed thoroughly. HOMO-LUMO energy gap with 4.27eV indicates that compound **3d** with pyrazolo-triazolo-pyrimidine rings has a good chemical stability and reactivity. However, lowering of HOMO-LUMO energy gap of **3d** derivative compared to intermediaries **1** and **2** clearly explains the charge transfer interactions taking place within the molecule which leads to its enhanced bioactivity. The molecular electrostatic potential has been mapped for predicting sites and relative reactivities towards electrophilic and nucleophilic attack which may have an influence in the antibacterial potential.

Acknowledgments

The authors are grateful to the Ministry of Higher Education and Scientific Research of Tunisia for financial support. The authors also extend their appreciation to the Deanship of Scientific Research at King Saud University for funding this work through the research group RG-164.

Appendix A. Supplementary data

Supplementary data to this article can be found online at https://doi.org/10.1016/j.molstruc.2019.127007.

References

[1] I. Filali, M.A. Belkacem, A. Ben Nejma, J.P. Souchard, H.B. Jannet, J. Bouajila, J. Enzym. Inhib. Med. Chem. 31 (2016) 1475–6374.
[2] A.V. Popov, V.A. Kobelevskaya, L.I. Larina, G.G. Levkovskaya, Mendeleev Commun. 27 (2017) 178–179.
[3] S.M. Riyadh, T.A. Farghaly, M.A. Abdallah, M.M. Abdalla, M.R. Abd El-Aziz, Eur. J. Med. Chem. 45 (2010) 1042–1050.
[4] B.A. Bhat, K.L. Dhar, S.C. Puri, A.K. Saxena, M. Shanmugavel, G.N. Qazi, Bioorg. Med. Chem. Lett 15 (2005) 3177–3180.
[5] A. Padmaja, C. Rajasekhar, A. Muralikrishna, V. Padmavathi, Eur. J. Med. Chem. 46 (2011) 5034–5038.
[6] K.C. Ragenovic, V. Dimova, V. Kakurinov, D.G. Molnar, A. Buzarovska, Molecules 6 (2001) 815–824.
[7] M.N.M. Yousif, W.A. El-Sayed, H.S. Abbas, H.M. Awad, N.M. Yousif, J. Appl. Pharm. Sci. 7 (2017) 21–32.
[8] W.A. El-Sayed, A.A.H. Abdel-Rahman, M.M.M. Ramiz, Z. Naturforschung 64c (2009) 323–328.
[9] E.P. Da, S. Falcao, S.J. De Melo, R.M. Srivastava, M.T.J. De, A. Catanho A, S.C.D. Nascimento, Eur. J. Med. Chem. 41 (2006) 276–282.
[10] O.A. Fathalla, I.F. Zeid, M.E. Haiba, A.M. Soliman, S.I. Abd-Elmoez, W.S. El-Serwy, World J. Chem. 4 (2009) 127–132.
[11] N. Singh, S.K. Pandey, R.P. Tripathi, Carbohydr. Res. 345 (2010) 1641–1648.
[12] W. Zhang, Z. Li, M. Zhou, F. Wu, X. Hou, H. Luo, H. Liu, X. Han, G. Yan, Z. Ding, R. Li, Bioorg. Med. Chem. Lett 24 (2014) 799–807.
[13] M. Zayane, A. Rahmouni, M. Daami-Remadi, M. Ben Mansour, A. Romdhane, H.B. Jannet, J. Enzym. Inhib. Med. Chem. 31 (2016) 1566–1575.
[14] M. Rafiq, M. Saleem, M. Hanif, S.K. Kang, S.Y. Seo, K.H. Lee, Arch Pharm. Res. (Seoul) 39 (2016) 161–171.
[15] K. Odlo, J. Hentzen, J.F. Chabert, S. Ducki, O.A.B.S.M. Gani, I. Sylte, M. Skrede, V.A. Fløtenes, T.V. Hansen, Bioorg. Med. Chem. 16 (9) (2008) 4829–4838.
[16] H. Brahmbhatt, M. Molnar, V. Pavic, Karbala Int. J. Mod. Sci. 4 (2018) 1–7.
[17] M.N. Ahmed, K.A. Yasin, S. Hameed, K. Ayub, I. Haq, M.N. Tahir, T. Mahmood, J. Mol. Struct. 1129 (2017) 50–59.
[18] M. Nadeem, U. Yunus, M.H. Bhatti, K. Ayub, M. Mehmood, M.J. Saif, J. Phys. Chem. Solids 110 (2017) 218–226.
[19] M.N. Ahmed, B. Sadiq, N.A. Al-Masoudi, K.A. Yasin, S. Hameed, T. Mahmood, K. Ayub, M.N. Tahir, J. Mol. Struct. 1155 (2018) 403–413.
[20] G. Ahmad, N. Rasool, H.M. Ikram, S.G. Khan, T. Mahmood, K. Ayub, M. Zubair, E. Al-Zahrani, U.A. Rana, M.N. Akhtar, N.B. Alitheen, Molecules 22 (2017) 190–209.
[21] A.E. Rashad, A.H. Shamroukh, M.I. Hegab, H.M. Awad, Acta Chim. Slov. 52 (2005) 429–434.
[22] A. Marmonier, Antibiotiques Technique de diffusion en gélose méthode des disques. Bactériologie médicale Techniques usuelles, SIMEP SA-Paris, France, 1987, pp. 237–243.
[23] A. Jabrane, H. Ben Jannet, M. Mastouri, Z. Mighri, J. Casanova, Nat. Prod. Res. 24 (2010) 491–499.
[24] R. Dennington, T. Keith, J. Millam, Gauss View, Version 5, Semichem Inc., Shawnee Mission KS,, 2009.
[25] M.J. Frisch, G.W. Trucks, H.B. Schlegel, Gaussian 09, Revision E.01, Gaussian Inc, Wallingford, CT, 2009.
[26] M.J. Bottomley, E. Muraglia, R. Bazzo, A. Carfi, J. Biol. Chem. 282 (2007) 13592–13600.
[27] O. Trott, A.J. Olson, J. Comput. Chem. 31 (2010) 455–461.
[28] A. Rahmouni, A. Romdhane, A. Ben Said, K. Majouli, H. Ben Jannet, Turk. J. Chem. 38 (2014) 210–221.
[29] A. Ben Said, A. Romdhane, A. Rahmouni A, A. Nguir, H. Ben Jannet, J. Adv. Chem. 10 (2014) 3254–3262.
[30] S.S. Medimagh, A. Romdhane, R.M. Daami, K.H. Jabnoun, D. Touboul, H. Ben Jannet, M.A. Hamza, Med. Chem. Res. 24 (2015) 3247–3257.
[31] A.M. El-Agrody, H.S. Abd-Rabboh, A.M. Al-Ghamdi, Med. Chem. Res. 22 (2013) 1339–1355.
[32] A. Rahmouni, A. Romdhane, A.B. Said, K. Majouli, H.B. Jannet, Turk. J. Chem. 38 (2014) 210–221.

[33] A. Rahmouni, S. Souiei, M.A. Belkacem, A. Romdhane, J. Bouajila, H.B. Jannet, Bioorg. Chem. 66 (2016) 160–168.
[34] C. Kim, J. Kim, H.Y. Park, H.J. Park, J.H. Lee, C.K. Kim, J. Yoon, Microbiol. Biotechnol. 80 (2008) 37–47.
[35] W. Kohn, A.D. Becke, R.G. Parr, J. Phys. Chem. 100 (1996) 12974–12980.
[36] Y.M. Álvarez-Ginarte, L.A. Montero-Cabrera, J.M. García de la Vega, P.N. Marín, Y. Marrero-Ponce, J.A. Ruíz-García, J. Steroid Biochem. Mol. Biol. 126 (2011) 35–45.
[37] X.H. Liu, L. Pan, C.X. Tan, J.Q. Weng, B.L. Wang, Z.M. Li, Asian J. Chem. 23 (2011) 4031–4036.
[38] B. Kosar, C. Albayrak, Spectrochim. Acta 78 (2011) 160–167.
[39] A.M. Asiri, M. Karabacak, M. Kurt, K.A. Alamry, Spectrochim. Acta 82 (2011) 444–455.
[40] H. Tanak, Int. J. Quantum Chem. 112 (2012) 2392–2402.
[41] M.J. Alam, S. Ahmad, Spectrochim. Acta A Mol. Biomol. Spectrosc. 96 (2012) 992–1004.
[42] M.J. Alam, S. Ahmad, Spectrochim. Acta A Mol. Biomol. Spectrosc. 136 (2015) 961–978.
[43] M.J. Alam, S. Ahmad, Spectrochim. Acta A Mol. Biomol. Spectrosc. 128 (2014) 653–664.
[44] H. Khanam, A. Mashrai, N. Siddiqui, M. Ahmad, M.J. Alam, S. Ahmad, Shamsuzzaman, J. Mol. Struct. 1084 (2015) 274–283.
[45] B. Kosar, C. Albayrak, Spectrochim. Acta A Mol. Biomol. Spectrosc. 78 (2011) 160–167.
[46] L.W. Li, C.J. Wu, Z.Q. Wang, L.X. Zhao, Z. Li, C.S. Sun, T.M. Sun, Spectrochim. Acta A. 136 (2015) 338–346.
[47] G. Subhapriya, S. Kalyanaraman, N. Surumbarkuzhali, S. Vijayalakshmi, V. Krishnakumar, J. Mol. Struct. 1083 (2015) 48–56.